Blocking CXCR4 alleviates desmoplasia, increases T-lymphocyte infiltration, and improves immunotherapy in metastatic breast cancer

Blocking CXCR4 alleviates desmoplasia, increases T-lymphocyte infiltration, and improves immunotherapy in metastatic breast cancer

Ivy X. Chen[a,b,c], Vikash P. Chauhan[a,b], Jessica Posada[a,d], Mei R. Ng[a], Michelle W. Wu[a], Pichet Adstamongkonkul[c], Peigen Huang[a], Neal Lindeman[d], Robert Langer[b,e], and Rakesh K. Jain[a,1]

[a]Edwin L. Steele Laboratories, Department of Radiation Oncology, Massachusetts General Hospital and Harvard Medical School, Boston, MA 02114; [b]Koch Institute for Integrative Cancer Research, Massachusetts Institute of Technology, Cambridge, MA 02139; [c]Harvard School of Engineering and Applied Sciences, Harvard University, Cambridge, MA 02138; [d]Department of Pathology, Brigham and Women's Hospital, Boston, MA 02115; and [e]Department of Chemical Engineering, Massachusetts Institute of Technology, Cambridge, MA 02139

Contributed by Rakesh K. Jain, December 7, 2018 (sent for review September 10, 2018; reviewed by Douglas T. Fearon and George W. Sledge)

Metastatic breast cancers (mBCs) are largely resistant to immune checkpoint blockade, but the mechanisms remain unclear. Primary breast cancers are characterized by a dense fibrotic stroma, which is considered immunosuppressive in multiple malignancies, but the stromal composition of breast cancer metastases and its role in immunosuppression are largely unknown. Here we show that liver and lung metastases of human breast cancers tend to be highly fibrotic, and unlike primary breast tumors, they exclude cytotoxic T lymphocytes (CTLs). Unbiased analysis of the The Cancer Genome Atlas database of human breast tumors revealed a set of genes that are associated with stromal T-lymphocyte exclusion. Among these, we focused on *CXCL12* as a relevant target based on its known roles in immunosuppression in other cancer types. We found that the CXCL12 receptor CXCR4 is highly expressed in both human primary tumors and metastases. To gain insight into the role of the CXCL12/CXCR4 axis, we inhibited CXCR4 signaling pharmacologically and found that plerixafor decreases fibrosis, alleviates solid stress, decompresses blood vessels, increases CTL infiltration, and decreases immunosuppression in murine mBC models. By deleting *CXCR4* in αSMA$^+$ cells, we confirmed that these immunosuppressive effects are dependent on CXCR4 signaling in αSMA$^+$ cells, which include cancer-associated fibroblasts as well as other cells such as pericytes. Accordingly, CXCR4 inhibition more than doubles the response to immune checkpoint blockers in mice bearing mBCs. These findings demonstrate that CXCL12/CXCR4-mediated desmoplasia in mBC promotes immunosuppression and is a potential target for overcoming therapeutic resistance to immune checkpoint blockade in mBC patients.

tumor microenvironment | metastatic breast cancer | immune checkpoint blockade | tumor desmoplasia | carcinoma-associated fibroblasts

Although recent clinical trials have reported durable responses in some metastatic breast cancer (mBC) patients receiving programmed cell death-1 (PD-1) or programmed cell death-ligand 1 (PD-L1) inhibitors, particularly in patients with triple-negative breast cancer, the overall response rate to immune checkpoint blockade (ICB) is still limited compared with success rates in other malignancies (1, 2). The mechanisms underlying poor response of mBC to novel immunotherapies are largely unclear. A hallmark of some other nonresponsive tumors, such as pancreatic ductal adenocarcinomas, is desmoplasia. These tumors are highly fibrotic-rich in cancer-associated fibroblasts (CAFs) and extracellular matrix (ECM) (3–6).

The fibrotic state can cause immunosuppression through multiple mechanisms. TGF-β1, an immunosuppressor promoted by tumor hypoxia, is known to drive matrix production by CAFs and to promote exclusion of T lymphocytes from tumors (7, 8). Specifically, FAP-expressing CAFs repel T lymphocytes from penetrating into tumors. This exclusion of T lymphocytes by CAFs may be driven in part by CXCL12/CXCR4 signaling (9). The dense collagen matrix produced by CAFs may also present a physical barrier to the infiltration of T lymphocytes (10, 11). Furthermore, mechanical compression of tumor blood vessels through buildup of physical pressure, termed "solid stress," by CAFs and matrix leads to tissue hypoxia and low pH (12, 13). Hypoxia and/or low pH can preferentially promote T-regulatory cell (Treg) infiltration and activity, increase the expression of immune checkpoint proteins such as PD-L1, and suppress the activity of T lymphocytes (14–18).

While fibrosis has been extensively investigated in primary breast tumors (10), there is a paucity of knowledge about the tumor microenvironment (TME) in metastatic lesions. Moreover, it remains unclear whether desmoplastic stroma contributes to immune suppression in mBC. The choice of therapy for mBC is typically based on pathological assessment of primary tumors;

Significance

Although immune checkpoint blockade (ICB) along with nab-paclitaxel has increased progression-free survival in triple-negative breast cancer patients, a large fraction of metastatic breast cancer (mBC) patients do not benefit from ICBs. The presence of a fibrotic tumor microenvironment can suppress the immune response to cancer. Here we found fibrosis and immunosuppression in both primary and metastatic breast cancer lesions. We show that targeting CXCR4/CXCL12 signaling, using plerixafor, an Food and Drug Administration-approved drug, reduces fibrosis, alleviates immunosuppression, and significantly enhances the efficacy of immune checkpoint blockers in preclinical models of mBC. Our findings provide a deeper understanding of mechanisms by which desmoplasia promotes immunosuppression in mBC and suggest a clinically translatable approach that can be combined with immunotherapy in patients to enhance therapeutic response.

Author contributions: I.X.C., V.P.C., M.R.N., P.A., P.H., R.L., and R.K.J. designed research; I.X.C., V.P.C., J.P., M.R.N., M.W.W., and P.A. performed research; I.X.C., J.P., P.H., N.L., R.L., and R.K.J. contributed new reagents/analytic tools; I.X.C., V.P.C., J.P., M.R.N., M.W.W., P.A., N.L., and R.K.J. analyzed data; and I.X.C., V.P.C., M.R.N., R.L., and R.K.J. wrote the paper.

Reviewers: D.T.F., Cold Spring Harbor Laboratory; and G.W.S., Stanford University Medical Center.

Conflict of interest statement: R.K.J. received an honorarium from Amgen; consultant fees from Merck, Ophthotech, Pfizer, SPARC, SynDevRx, and XTuit; owns equity in Enlight, Ophthotech, and SynDevRx; and serves on the Boards of Trustees of Tekla Healthcare Investors, Tekla Life Sciences Investors, Tekla Healthcare Opportunities Fund, and Tekla World Healthcare Fund. Neither any reagent nor any funding from these organizations was used in this study. R.K.J. and D.T.F. are co-authors of a 2018 National Cancer Institute-Tumor Immune Microenvironment Workshop meeting report.

[1]To whom correspondence should be addressed. Email: jain@steele.mgh.harvard.edu.

This article contains supporting information online at www.pnas.org/lookup/suppl/doi:10.1073/pnas.1815515116/-/DCSupplemental.

Published online January 30, 2019.

thus, poor response rates for metastatic disease may in part be due to differences between the primary and metastatic TME (19).

In this study, we first performed unbiased analysis of the The Cancer Genome Atlas (TCGA) database on human breast cancer and found CXCL12/CXCR4 signaling as a potential T cell exclusion mechanism in mBC. By analyzing paired biopsies of primary and metastatic legions, we then confirmed that CXCR4 expression correlates with desmoplasia and immunosuppression in both human primary and metastatic breast tumors. To reveal the underlying mechanisms, we employed preclinical models of mBC and found that inhibiting CXCL12/CXCR4 signaling or deleting *CXCR4* in aSMA+ cells alleviates desmoplasia and reduces immunosuppression in mBC. Finally, we demonstrated that pharmacological inhibition of CXCR4—using an FDA-approved drug plerixafor (AMD3100)—significantly decreases the development of spontaneous lung metastasis and sensitizes the mBC tumors to immune checkpoint blockers.

Results

CXCL12/CXCR4 Axis Is a Potential Mediator of Cytotoxic T-Lymphocyte Exclusion in Human Breast Cancer. To understand the potential mechanisms that may contribute to immunosuppression in mBC and to identify potential targets for intervention, we first analyzed human breast cancer (BC) gene expression data from TCGA (20). We identified genes the expression of which is strongly correlated with genes connected with T-lymphocyte exclusion in cancer—*TGFB1*, *FAP*, and *COL1A1* (7–9). We found that 1,207 genes correlated with *TGFB1*, 785 with *FAP*, and 727 with *COL1A1* (Datasets S1–S3). Among these highly correlated genes, 273 genes overlapped (Fig. 1*A*). Gene Ontology

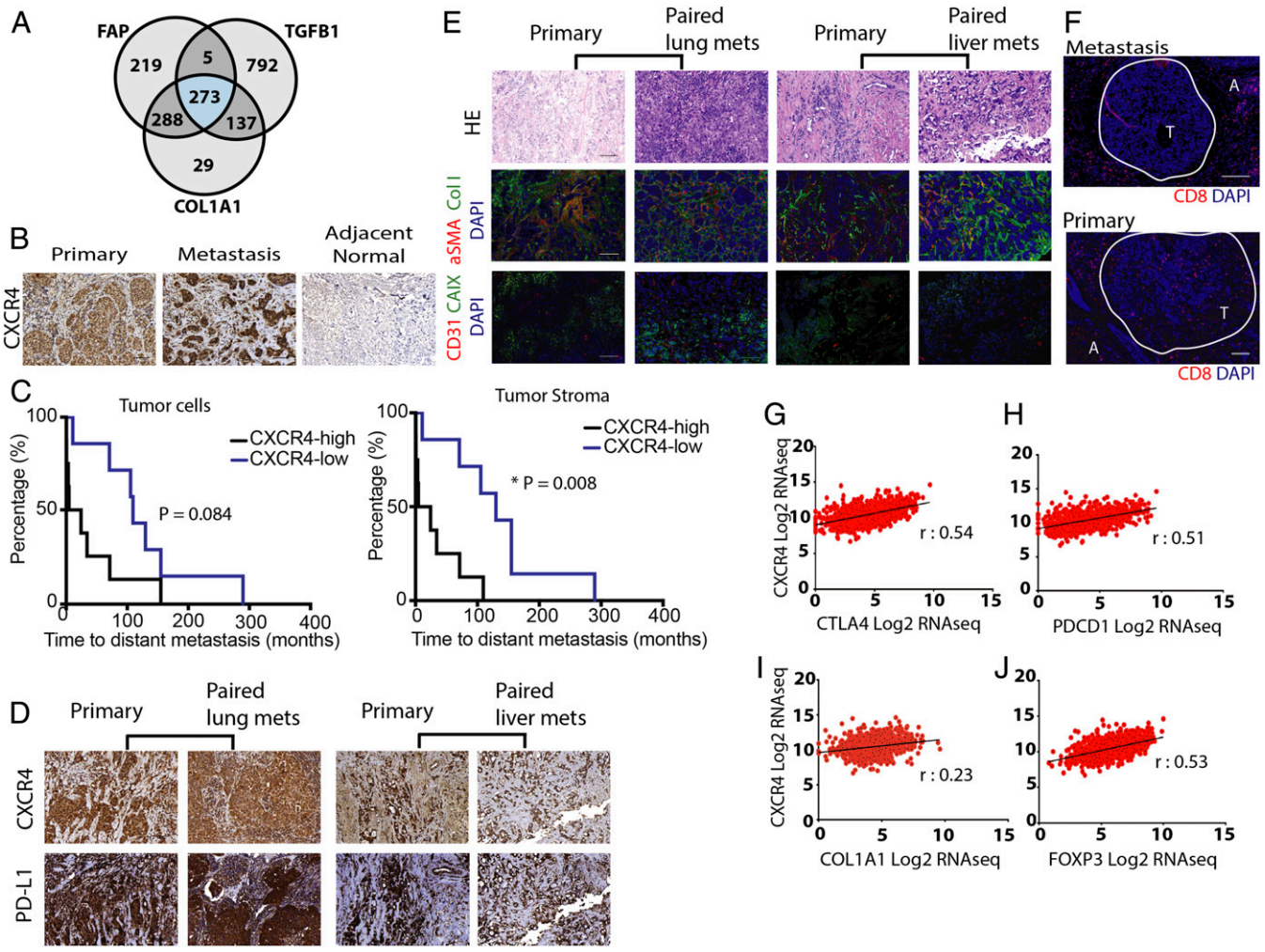

Fig. 1. CXCR4 is strongly correlated with desmoplasia- and immune checkpoint-related gene and protein expression in human breast cancers. (*A*) Venn diagram of the number of genes associated with FAP, TGFB1, and COL1A1 from breast invasive carcinoma mined from the human breast cancer TCGA database. (*B*) Immunohistochemistry (IHC) staining of human formalin-fixed paraffin-embedded (FFPE) tissues for CXCR4 in primary tumor, metastatic lesions, and adjacent normal tissues. CXCR4 is overexpressed in both primary and metastatic human breast tumors, compared with normal tissues. (*C*, *Left*) Kaplan–Meier survival analysis of patients stratified by high CXCR4 expression (>70%) vs. low expression in cancer-cell–rich regions of the tumor (log-rank $P = 0.084$). (*C*, *Right*) Kaplan–Meier survival analysis of patients stratified by high stromal CXCR4 expression (>30%) vs. low expression (* log-rank $P = 0.008$; $n = 17$). (*D*) IHC images showing CXCR4 and PD-L1 in matched pairs of primary and metastatic human BC tissues (*Left*, lung metastases; *Right*, liver metastasis). Both primary and metastatic tissues show high levels of CXCR4 and PD-L1, enriched in tumor stromal regions. (*E*) Representative IHC staining of human FFPE tissues with CD31, CAIX, aSMA, and Collagen I in matched pairs of primary and metastatic BC tissues (*Left*, lung metastases; *Right*, liver metastases). Both primary and metastatic tissues show high level of fibrosis. H&E staining of corresponding regions are shown. (*F*) Representative IHC staining of CD8+ T cells in primary and metastatic BC tissues. A, adjacent normal tissue; T, tumor region (circled in white). (*G–J*) Pearson correlation coefficients of CXCR4 mRNA expression from the TCGA BRCA dataset with immune checkpoint markers (*G*) CTLA4 ($r = 0.54$, $P < 0.0001$) and (*H*) PDCD1 ($r = 0.51$, $P < 0.0001$), desmoplasia marker (*I*) COL1A1 ($r = 0.23$, $P < 0.001$), and Treg marker (*J*) FOXP3 ($r = 0.53$, $P < 0.001$), combined from all BC patients ($n = 1,215$). (Scale bar, 100 μm.)

analysis of the overlapping genes revealed enrichment for genes in the pathway "regulation of cell migration" as a top hit (Dataset S4), indicating potential genes that may affect T-lymphocyte infiltration into mBC tumors. We found that 38 of the 273 genes were among this category. Among these genes, *CXCL12* has been implicated in immunosuppression through its receptor CXCR4 in other cancers (9, 21–23). Targeting the CXCL12/CXCR4 pathway increased antitumor immunity largely by reducing intratumoral FoxP3+ Tregs (21, 22) and improved the outcome of PD-1 blockade in murine models of pancreatic and liver cancers (9, 21).

CXCR4 Correlates with Desmoplasia and Immunosuppression in Human mBC. To determine whether CXCR4 expression differs in primary versus metastatic tumors, we next examined the TME in paired primary and metastatic lesion biopsies from 17 mBC patients (10 primary/liver metastases and 7 primary/lung metastases). We found that CXCR4 was highly expressed in both metastatic sites, compared with normal tissues (Fig. 1*B* and *SI Appendix*, Fig. S1*A*). Although CXCR4 expression levels were similar in both primary tumor and metastatic lesions, there was a significant correlation between the two sites in paired cases (*SI Appendix*, Fig. S1 *A* and *B*). In addition, high expression of cancer (>70%) and stromal (>30%) CXCR4 was indicative of shorter progression-free survival in these patients (Fig. 1*C*). We also found strong colocalization of CXCR4 and PD-L1 expression in both primary tumor and liver or lung metastases from the same patients (Fig. 1*D* and *SI Appendix*, Fig. S1*C*). There was also higher expression of PD-L1 in the metastatic lesions compared with primary tumors; however, there was no correlation between the two sites, indicating that higher expression of PD-L1 in the primary tumor did not necessarily confer higher expression in the metastases (*SI Appendix*, Fig. S1 *D* and *E*). Furthermore, we histologically assessed these samples for CD8+ cytotoxic T-lymphocyte (CTL) infiltration and found that the metastatic lesions are largely devoid of CTLs (Fig. 1*F*). Although there was a trend toward a negative correlation between CXCR4 and CD8 expression, it was not significant (*SI Appendix*, Fig. S1*F*). We also found that the metastatic lesions are enriched in CAFs and collagen I and are hypoxic (Fig. 1*E* and *SI Appendix*, Fig. S2). Further analysis of TCGA gene expression data also indicated a strong positive association between *CXCR4* expression and desmoplastic and immunosuppressive markers such as *COL1A1*, *CTLA4*, *PDCD1*, and *FOXP3* (Fig. 1 *G*–*J*). The correlation was consistent regardless of the tumor subtypes, as well as in node-positive mBC (*SI Appendix*, Fig. S3). Collectively, these findings suggest that CXCL12/CXCR4 signaling could play an important role in promoting fibrosis and immunosuppression in both the primary and metastatic TME of mBC.

CXCR4 Inhibition Decreases CAF Recruitment, Desmoplasia, and Solid Stress in a Mouse Model of BC. Next we sought to determine whether AMD3100—a CXCR4 blocker—could be used to reduce fibrosis and immunosuppression in mBC. Expression of CXCR4 has been shown to be elevated in CAFs isolated from primary human breast tumors (23). We first examined whether CXCR4 plays a role in the recruitment of CAFs to tumors in a mouse model of BC that recapitulates the fibrosis observed in human HER2+ BC (MCa-M3C; derived from a *MMTV-PyVT* spontaneous BC mouse model). We implanted mammary fat pad windows in transgenic reporter mice expressing αSMA promoter-driven DsRed to mark activated CAFs, realizing that a small population of other cells such as pericytes also express αSMA (24–26). We then implanted these mice with CFP-labeled MCa-M3C cells and treated them with saline (control) or AMD3100 through continuous infusion using osmotic pumps (21). Using time-lapse imaging with intravital multiphoton microscopy, we found that AMD3100 reduced the accumulation of αSMA+ cells in the TME to a greater degree than saline (control) (Fig. 2*A*). Accumulation of αSMA+ cells started around day 3 posttumor implantation in control mice, while such recruitment was largely delayed in the treatment mice. We next orthotopically implanted MCa-M3C tumor cells in wild-type FVB mice, treated these mice with AMD3100 or saline, and

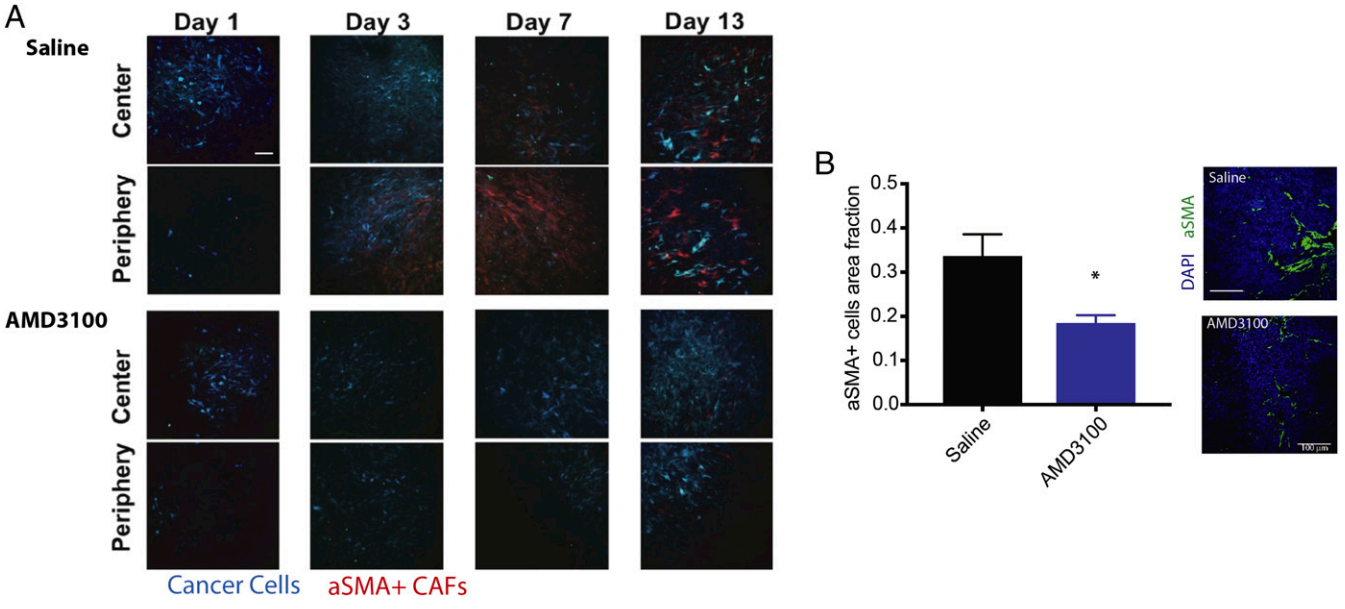

Fig. 2. Inhibition of CXCR4 reduces stromal αSMA+ cells in tumors. (*A*) αSMA-dsRed mice bearing mammary fat pad windows were implanted with MCa-M3C-CFP breast tumors. Representative time-lapse images from intravital multiphoton microscopy of cancer cells (blue) and αSMA+ cells (red) at days 1, 3, 7, and 13 postimplantation and during treatment of AMD3100 or saline (control). CXCR4 inhibition delays the accumulation of αSMA+ cells at both the center and periphery of the tumors. (Scale bar, 100 μm.) (*B*) Area fractions and representative histology images of tumor αSMA+ cells show that AMD3100 reduces density of αSMA+ cells in the tumors (*$P < 0.05$, Student's *t* test). (Scale bar, 100 μm.)

then isolated the tumors at day 10 posttreatment to evaluate whether inhibition of αSMA+ cell recruitment through CXCR4 can reduce fibrosis (Fig. 3 *A–D*). We histologically confirmed the reduction of αSMA+ cell density in AMD3100-treated mice (Fig. 2*B*). CAFs in desmoplastic tumors generate a type of pressure called solid stress and transmit this pressure through the matrix to compress blood vessels (12). This vessel compression resulting from desmoplasia can lower drug and oxygen delivery (13, 27). We measured solid stress using the bulk tumor opening method (12) and found that AMD3100 significantly reduced solid stress levels (Fig. 3*A*). AMD3100 treatment also decompressed tumor blood vessels (Fig. 3*B*) without increasing vessel density (*SI Appendix*, Fig. S4*A*), indicating an increase in perfusion. Decompressing existing collapsed blood vessels is known to decrease tumor hypoxia (13). Indeed, we found that AMD3100 treatment decreased hypoxia, measured using pimonidazole staining (Fig. 3*C*). Moreover, AMD3100 treatment substantially lowered collagen I and hyaluronan expression (Fig. 3*D* and *SI Appendix*, Fig. S4 *B* and *C*) compared with the control.

CXCR4 Inhibition Decreases Profibrotic and Immunosuppressive Gene Expression in Mouse Models of BC. To understand how CXCR4 inhibition might affect tumor fibrosis and immunosuppression, we performed qRT-PCR on RNA extracted from MCa-M3C tumors treated with AMD3100 or control. Consistent with our observation of a reduction of CAF recruitment and activity, we found that CXCR4 inhibition significantly reduced several markers of desmoplasia (*Cxcr4*, *Tgfb*, *Ctgf*, *Edn1*) (Fig. 3*E*). We confirmed similar results in a second syngeneic model of triple-negative mBCs, E0771 (*SI Appendix*, Fig. S5*A*). We also analyzed the gene expression levels of various immunomodulatory chemokines and cytokines in the MCa-M3C tumors using a qRT-PCR array and confirmed the top hits by qRT-PCR (Fig. 3*F*). Treatment with AMD3100 increased expression of *Ifng* and *Gzmb* (Fig. 3*F*), which are known to be critical for antitumor immunity (28). Notably, we found that AMD3100 reduced expression of *Cxcl5* and *Cxcr2* (Fig. 3*F* and *SI Appendix*, Fig. S5*B*), which have been implicated in promoting lung metastases in mBC (29–31). We also found that, although the fractions of intratumoral CD8a+ T cells were similar between the groups, there was a decrease in the infiltration of FoxP3+ regulatory T cells in tumors treated with AMD3100 (*SI Appendix*, Fig. S6). To test whether this change in immune-related factors can be attributed to CAFs, we implanted orthotopic MCa-M3C tumors into transgenic *αSMA-DsRed* mice and treated the mice with AMD3100 or saline (control) for 10 d. The immunosuppressive subtype of CAFs express high levels of both αSMA and FAP in human breast cancers (32); therefore, we also evaluated the FAP+ CAFs in this model. We confirmed CXCR4 expression in the αSMA^+ cells, with FAP^+ cells expressing a negligible level of CXCR4 (*SI Appendix*, Fig. S7 *A* and *B*). Next we sorted out two populations of CAFs, $CD45^-dsRed^+$ (αSMA^+) and $CD45^-FAP^+$, and measured chemokine/cytokine gene expression in these CAFs using a qRT-PCR array. In both sorted CAF populations, we found decreased expression of *Cxcl5* (*SI Appendix*, Fig. S8). These data suggest that CXCR4 inhibition alleviates the fibrotic and immunosuppressive TME induced by CAFs and further reduces prometastatic signaling.

CXCR4 Blockade and αSMA^+ Cell-Specific CXCR4 Knockout Decreases Immunosuppression in BC. As the CXCL12/CXCR4 axis is a known driver of CAFs in breast cancer (32) and CAFs appear central to T-lymphocyte exclusion in bladder and colorectal cancers (7, 33), we next investigated the effects of αSMA^+ cell-specific

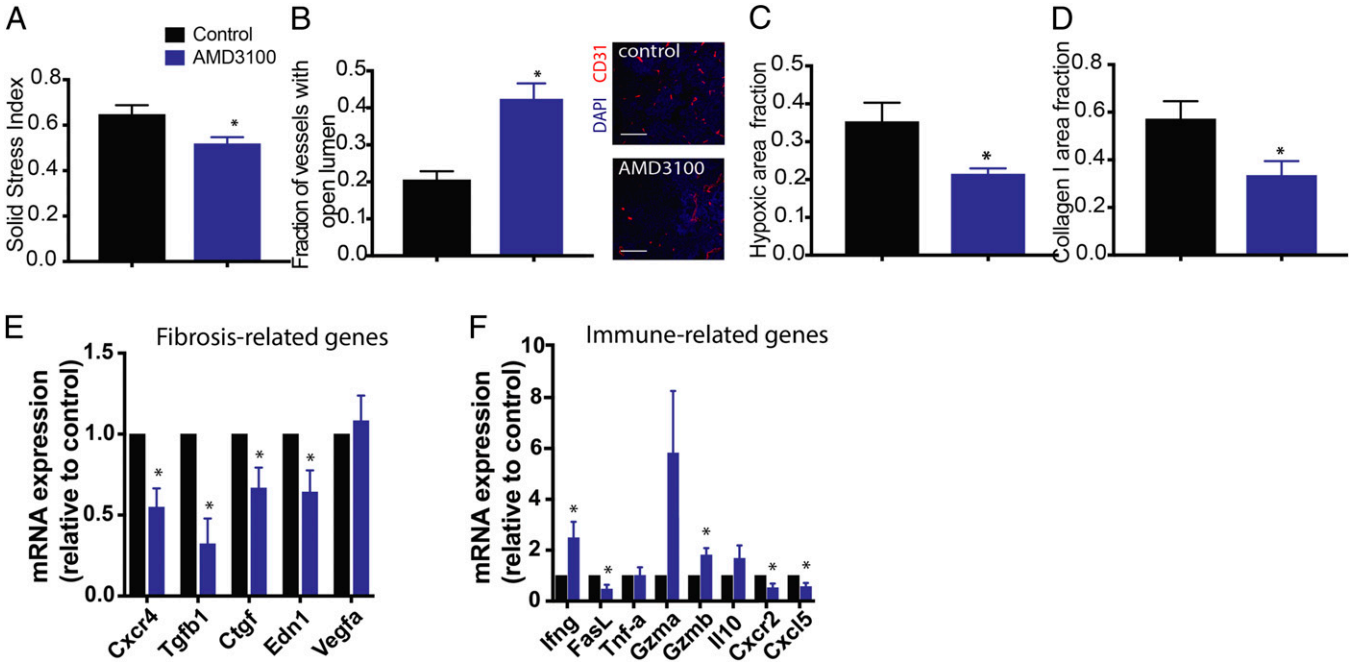

Fig. 3. Inhibition of CXCR4 reduces tumor desmoplasia and immunosuppression. (*A–D*) Histological and biomechanical quantification of orthotopic Mca-M3C tumors in mice treated with AMD3100 or saline ($n = 7$). (*A*) AMD3100 decreases relative solid stress level in BC tumors (*$P < 0.05$). (*B*) AMD3100 increases vessel decompression (*$P < 0.01$), as indicated by increased fractions of tumor blood vessels with open lumen, shown in representative images of tumor CD31+ vessels. (Scale bar, 100 μm.) (*C*) Quantification of hypoxic fractions in tumors measured by pimonidazole injection and staining shows that AMD3100 reduces tumor hypoxia (*$P < 0.05$). (*D*) Quantification of tumor collagen I area fractions shows that AMD3100 reduces expression of collagen I in the tumors (*$P < 0.05$). (*E* and *F*) Gene expression (qRT-PCR) analysis on whole tumors isolated from mice treated with AMD3100 or saline (control; n = 3–4). AMD3100 decreases fibrosis-related genes (*E*) and modulates expression of immune-related genes (*F*). Error bars indicate SEM. Analysis by unpaired two-sided Student's *t* test.

CXCR4 signaling in breast TME. To this end, we first confirmed there was expression of CXCR4 on CAFs in both primary and metastatic lesions (*SI Appendix*, Fig. S9). Therefore, we generated a αSMA$^+$ cell-specific conditional CXCR4 knockout mouse model of mBC. We crossed *Cxcr4$^{flox/flox}$* mice with those carrying a *Cre-ER^{T2}* transgene under control of the *αSMA* promoter to generate *αSMA-Cre-ER^{T2}/Cxcr4$^{flox/flox}$* mice (Fig. 4*A*). To induce knockout of Cxcr4 expression specifically in αSMA$^+$ cells, which largely represent CAFs, we injected tumor-naive mice daily with tamoxifen, the ER^{T2} agonist, for 2 wk before tumor implantation. We implanted orthotopic E0771 breast tumors into *αSMA-Cre-ER^{T2}/Cxcr4$^{flox/flox}$* or *Cxcr4$^{flox/flox}$* (control) mice from the same cohort. Flow cytometry analyses of tumors extracted at day 14 confirmed reduced expression of CXCR4 in αSMA+ cell populations in the tumors (Fig. 4*B*). The knockout mice had a reduced fraction of CXCR4+ αSMA+ cells compared with the control and to a greater degree than wild-type mice treated with the CXCR4 inhibitor AMD3100. Analysis by qPCR also validated decreased expression of *Cxcr4* and *Cxcl12* in the tumors (*SI Appendix*, Fig. S10*A*). We also observed a reduction in the total αSMA+ population in these tumors (*SI Appendix*, Fig. S10*B*).

To better understand how CXCR4 in CAFs might affect the immune microenvironment, we analyzed immune cell populations

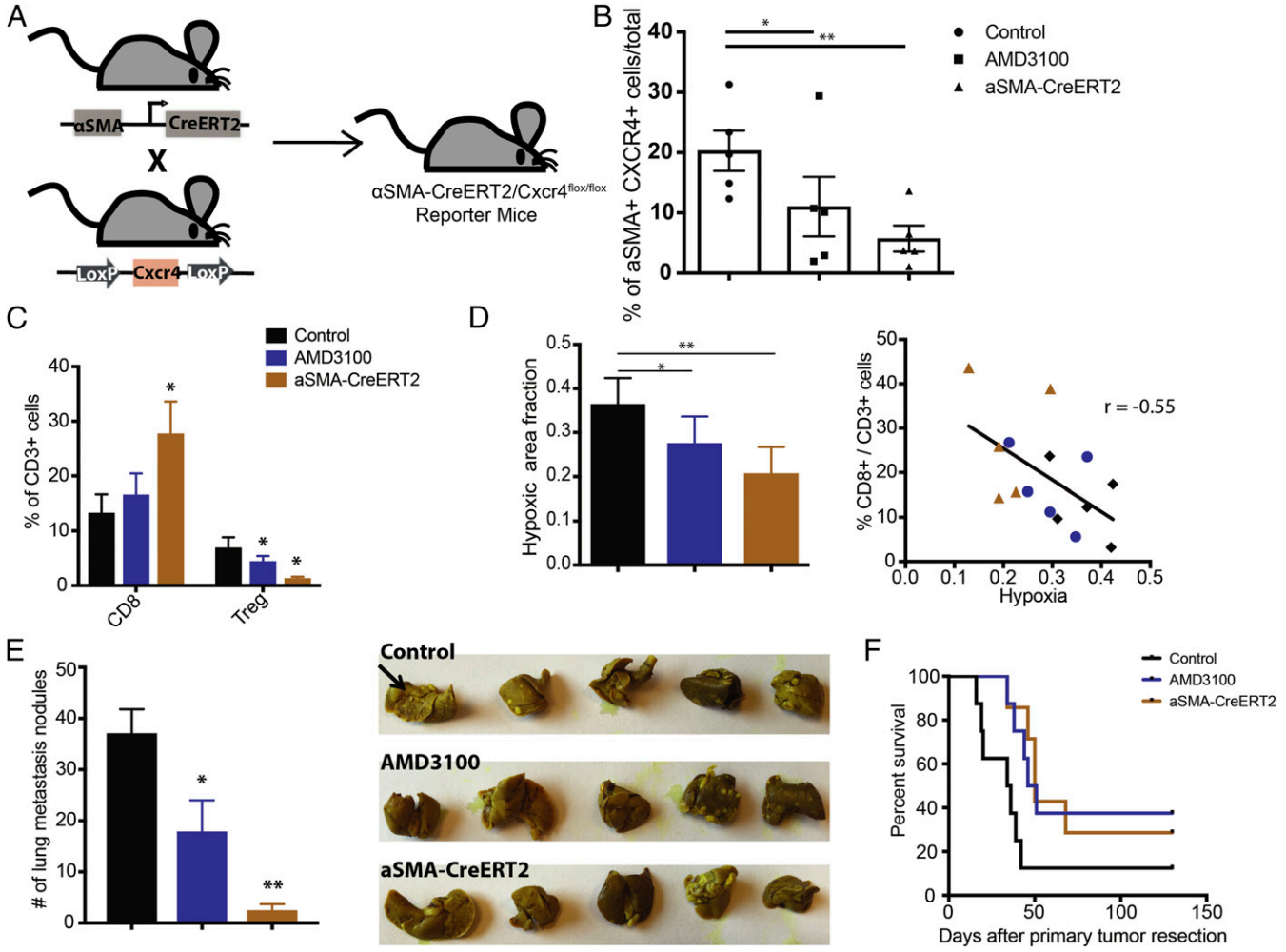

Fig. 4. Conditional deletion of CXCR4 in aSMA+ cells reduces immunosuppression and improves animal survival. (*A*) Schematic of generation of a αSMA-CreERT2/Cxcr4$^{flox/flox}$ mouse. Mice with CXCR4 alleles flanked by LoxP sites (Cxcr4$^{flox/flox}$) were bred with αSMA-CreERT2 mice expressing CreERT2 specifically in the αSMA+ cells to generate αSMA-CreERT2/Cxcr4$^{flox/flox}$ mice. (*B–F*) Conditional knockout of CXCR4 expression was induced by daily injection of tamoxifen (10 mg/kg) for 2 wk before tumor implantation (n = 5–8). Control mice also received tamoxifen. (*B*) Flow cytometry analysis of CXCR4+ αSMA+ expression level in E0771 breast tumors implanted in αSMA-CreERT2/Cxcr4$^{flox/flox\ mice}$, αSMA-CreERT2-negative (control), or wild-type mice. The wild-type mice were treated with AMD3100 via osmotic pumps for 2 wk. AMD3100 reduces the CXCR4+αSMA+ cell population (*P < 0.05), and the genetic deletion (αSMA-CreERT2) further decreases the population (**P < 0.01). (*C*) Flow cytometry analysis of cytotoxic lymphocytes (CD8) and regulatory T-lymphocyte (Treg) populations from orthotopic E0771 breast tumors. The αSMA-CreERT2/Cxcr4$^{flox/flox}$ mice have increased CD8+ cell fractions and decreased Treg cell fractions. *P < 0.05, by one-way ANOVA. (*D*, *Left*) Immunohistochemical analysis of hypoxia (pimonidazole injection) from orthotopic E0771 breast tumors is quantified. Both the AMD3100 treatment and genetic deletion (αSMA-CreERT2/Cxcr4$^{flox/flox}$) reduce hypoxic fractions of the tumors (*P = 0.049, **P = 0.0034, Student's t test). (*D*, *Right*) Linear regression analysis shows strong negative correlation between infiltration of CD8+ T cells and hypoxia (r = –0.55, P < 0.05; Pearson correlation). (*E*, *Left*) Quantification of the number of spontaneous lung metastatic nodules after primary (mammary fat pad) tumor resection at day 21. Both the AMD3100 treatment and genetic deletion reduce spontaneous metastasis formation in the lung (*P < 0.05, **P < 0.001, Student's t test). (*E*, *Right*) Representative gross images of lungs stained with Bouin's solution. Black arrow points to example of lung nodules. (*F*) Kaplan–Meier survival analysis of metastatic setting studies in mice with spontaneous lung metastases arising from orthotopic E0771 tumors. The mice were treated with saline (Cre-mice) or AMD3100 (wild-type) using an osmotic pump for 2 wk. Both AMD3100 treatment and genetic deletion improve animal survival (P < 0.05, by log-rank test). Error bars indicate SEM.

in these tumors by flow cytometry. Tumors from the *αSMA-Cre-ER^{T2}/Cxcr4$^{flox/flox}$* mice had increased numbers of cytotoxic CD8+ CTLs, decreased numbers of FoxP3+ Tregs, and an increased ratio of CTL to Tregs versus the control, indicating a reversal of immunosuppression (Fig. 4*C* and *SI Appendix*, Fig. S11). Moreover, histological analysis revealed substantially lower hypoxia in the tumors of *αSMA-Cre-ER^{T2}/Cxcr4$^{flox/flox}$* and AMD3100-treated mice (Fig. 4*D*). Notably, there was a strong inverse correlation between the infiltration of CD8 CTLs and hypoxia (Fig. 4*D*). Since CXCR4 has been shown to promote myeloid cell recruitment (34–36), we next analyzed tumor-infiltrating myeloid cells in the mice. There were no significant changes in the total myeloid cell population or the percentage of CD45+CD11b+Gr1+ myeloid-derived suppressor cells (*SI Appendix*, Fig. S12 *A* and *B*). However, there was a 50% reduction in CD11b+ Gr1+ Ly6G+ neutrophils in both CreERT2 and AMD3100-treated mice (*SI Appendix*, Fig. S12*C*). On the other hand, we observed a reduction in CD11b+ F4/80+ macrophages only in the AMD3100-treated mice (*SI Appendix*, Fig. S12*D*). These results suggest a potential mechanism of CAF-mediated recruitment of neutrophils to the TME via activation of CXCR4 signaling.

αSMA^{+} Cell-Specific CXCR4 Deletion Decreases Metastasis and Improves Survival in mBC. We next assessed the effects of silencing CAF-specific signaling on metastatic development. To examine spontaneous metastases formation, we implanted orthotopic E0771 breast tumors in the mice and resected the primary tumors once they reached a tumor diameter of 13 mm. Three weeks after primary tumor resection, we killed the mice and examined their lungs for metastatic nodules. There were significantly fewer lung metastases in both *αSMA-Cre-ER^{T2}/Cxcr4$^{flox/flox}$* and AMD3100-treated mice versus controls, with the highest reduction observed in the *αSMA-Cre-ER^{T2}/Cxcr4$^{flox/flox}$* group (Fig. 4*E*). Correspondingly, both genetic deletion and pharmacological blockade of CXCR4 also allowed for a moderate but significant extension of animal survival (Fig. 4*F*).

CXCR4 Blockade Improves T Cell Infiltration and Response to ICBs in mBC. Given that CXCR4 inhibition decreased fibrosis and immunosuppression, we assessed whether it could render the largely resistant mBCs responsive to ICB therapies. Since CXCR4 inhibitors effectively decreased spontaneous BC lung metastasis, we first investigated whether blocking CXCR4 signaling might have reprogrammed the metastatic tumor microenvironment,

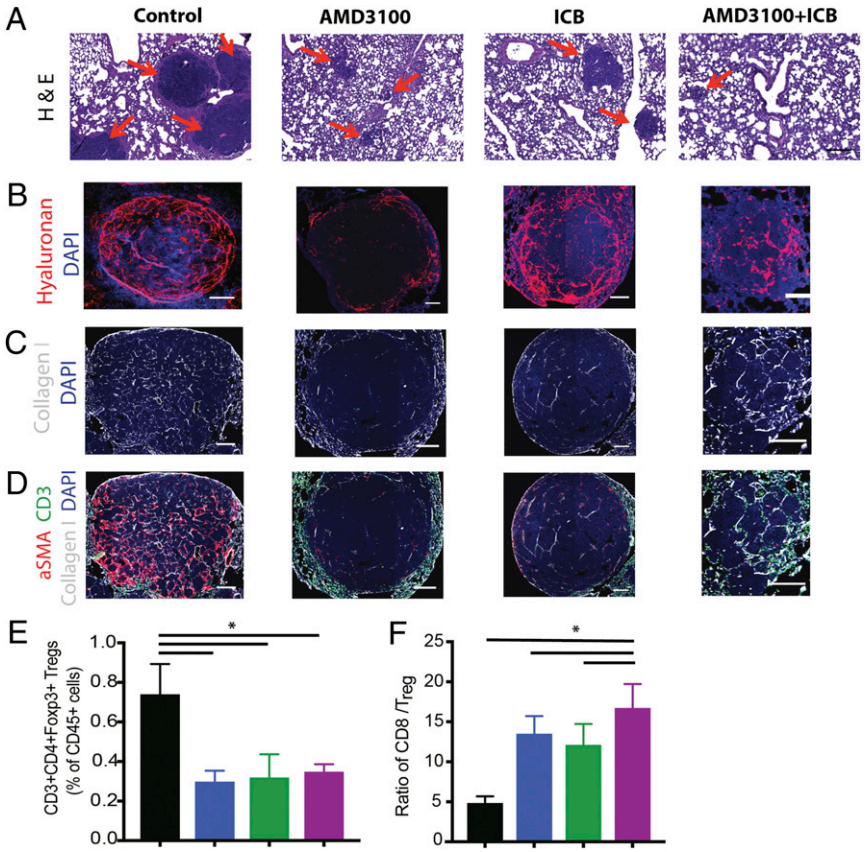

Fig. 5. Inhibition of CXCR4 reduces desmoplasia and increases effector to regulatory T-lymphocyte ratio in the lung metastases. (*A–D*) Representative histology images of lung metastases derived from orthotopic E0771 breast tumors. Immunofluorescence (IF) images of lung metastases were field-of-view images from the mosaic confocal imaging. After primary tumor resection, the mice were treated with AMD3100 in combination with an ICB mixture of α-CTLA-4 and α-PD-1 for one cycle, and the lung metastases were collected for analysis. (*A*) H&E stainings of spontaneous lung metastases from E0771 tumors. The metastatic nodules (red arrows) are significantly larger in the control, compared with all three treatment groups. (Scale bars, 100 μm.) (*B*) Representative images of IF staining of hyaluronan. Treatment with AMD3100 reduces the hyaluronan fraction in the metastatic TME. (*C*) Representative images of IF staining of collagen I. Treatment with AMD3100 reduces collagen I in the metastases. (*D*) Representative IF images showing aSMA (red), collagen I (white), and CD3 (green) in the metastases. Combination of AMD3100 and ICB increases infiltration of CD3+ cells into the TME. (*E* and *F*) Flow cytometry analysis of lung metastases derived from orthotopic E0771 breast tumors. (*E*) CD3+CD4+Foxp3+ regulatory T cell population. Both the monotherapy and combination therapy decrease Foxp3 T cells in the tumors (*P = 0.017, by one-way ANOVA). (*F*) CD8+ to Foxp3+ Treg ratio. Both AMD3100 groups increase the ratio of effector CD8+ T cells to Treg, and the combination of AMD3100 with immunotherapy mixture further extends the ratio (*P = 0.026, by one-way ANOVA). n = 5. Error bars indicate SEM. (Scale bar, 100 μm.)

with or without ICBs. To evaluate this, we implanted orthotopic MCa-M3C breast tumors in the mice, resected the primary tumors at a tumor diameter of 13 mm, and initiated treatment 1 wk postsurgery, when mBCs were established (based on our prior studies). We then treated the mice with a combination therapy of AMD3100 and a mixture of ICBs against the immune checkpoint cytotoxic T-lymphocyte–associated protein 4 (α-CTLA-4) and α-PD-1. Three weeks after primary tumor resection, we analyzed the lung metastatic nodules. Macroscopic observation revealed that the lung mBCs displayed significantly smaller metastatic nodules in the treatment groups (Fig. 5*A*). Furthermore, immunohistochemical analysis of the lung nodules showed that metastatic TME also presented with various levels of fibrosis, as indicated by strong deposition of collagen-I and hyaluronan (Fig. 5 *B* and *C*). In comparison, we found that treatment with AMD3100 and/or ICBs had lowered ECM expression levels in the metastatic nodules, possibly due to the smaller size of these metastases (37). Interestingly, we observed that in the metastases CD3 T lymphocytes were present mainly along the periphery of the tumors, displaying a T cell exclusion phenomenon (Fig. 5*D*) (9, 33). AMD3100 reduced αSMA+ cells and disrupted such physical exclusion and allowed more T cells to infiltrate into the TME when combined with ICB (Fig. 5*D*). This suggests that CXCR4 inhibition potentially facilitated the infiltration of T cells into contact with cancer cells and delayed metastatic growth.

We also profiled the immune cell populations from the metastases by flow cytometry. We found that AMD3100 treatment decreased the number of CD4+FoxP3+ Tregs and increased the ratio of CD8+ to CD4+ FoxP3+ cells (Fig. 5 *E* and *F* and *SI Appendix*, Fig. S13 *A* and *B*), while the ICB mixture also increased the CD8+ to Treg ratio. In addition, the combination of AMD3100 with ICBs showed greater reversal of immunosuppression than the monotherapy (Fig. 5 *E* and *F*). Although qRT-PCR analyses showed that AMD3100 alone did not alter cytokine expression in the metastases, the combination therapy of AMD3100 and ICBs increased the expression of several markers of T cell activity (*Ifng*, *Gzmb*, *Gzma*, *Tnfa*) while decreasing the expression of immunosuppressive markers (*Il10*, *Tgfb1*) and checkpoint molecules (*Tigit*, *Tim3*, *Pdl1*, *Pdcd1*, *Ctla4*) (*SI Appendix*, Fig. S13*C*), suggesting a shift to an immunostimulatory TME.

CXCR4 Inhibition Sensitizes Largely Resistant mBC Models to ICBs. Finally, we sought to test whether CXCR4 inhibition sensitizes mBCs to ICB. We tested the combination of AMD3100 with ICB therapy in the metastatic setting in three mBC mouse models: MCa-M3C (HER2+), E0771 (triple negative), and 4T1 (triple negative). We implanted orthotopic breast tumors in the mice, resected the primary tumors, and waited 3 (4T1) or 7 d (MCa-M3C and E0771) before treatment to allow established metastases to develop. CXCR4 inhibition increased response rates to ICBs and resulted in significantly fewer metastases in the lungs (Fig. 6 *A*–*C*). Monotherapy of AMD3100 alone provided moderate survival benefits in two of the models, MCa-M3C and E0771, but not in 4T1 (Fig. 6 *D*–*F*). In contrast, the combination therapy increased median survival of the mice bearing 4T1 tumors by 35%, with 2 long-term survivors of 10. The combination also extended the median animal survival by 76% (60 versus 34 d) for the mice with metastatic MCa-M3C, with 2 long-term survivors of 10. Furthermore, 57% of the mice with metastatic E0771 were disease-free for more than 6 mo after treatment of the combination therapy, extending from a median survival of 35 d in the control. This doubled the 29% cure rate for ICB treatment alone. Thus, these findings indicate that alleviating tumor desmoplasia and immunosuppressive TME with CXCR4 inhibition sensitizes models of immunotherapy-resistant mBC.

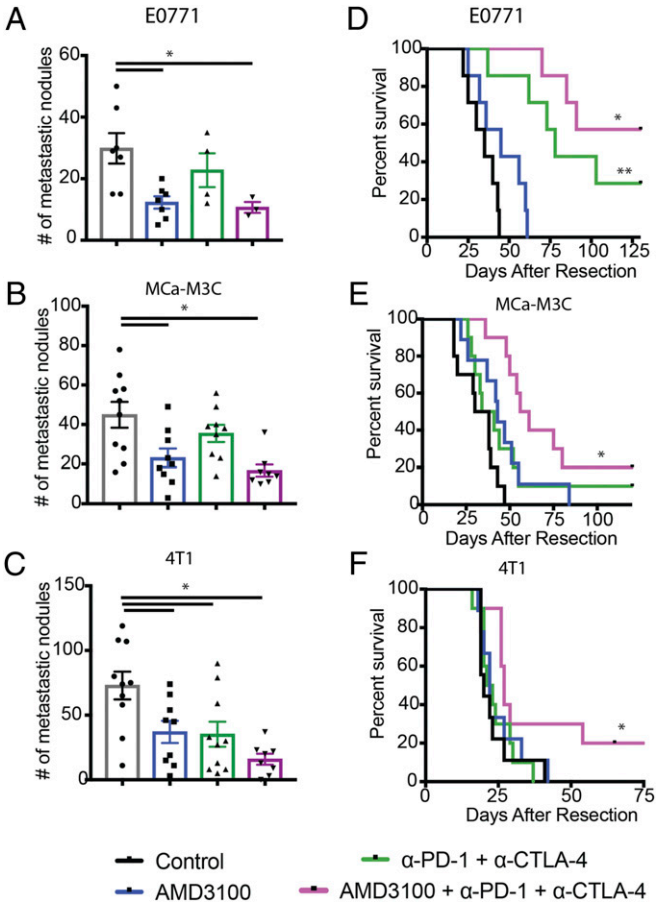

Fig. 6. CXCR4 inhibition improves outcome of ICBs. (*A*–*C*) Quantification of lung nodules in mice with spontaneous lung metastases arising from orthotopic breast tumors. Mice were treated with AMD3100 or saline (control) through an osmotic pump for 2 wk and with or without immune checkpoint blockades (α-CTLA-4 and α-PD-1) on days 2, 5, and 8. Lungs were collected and counted at the end point of the metastatic survival studies. Both AMD100 or combination therapy of AMD310 with immunotherapy mixture reduces metastatic nodules (E0771: $*P = 0.011$, MCa-M3C: $*P = 0.0018$, 4T1: $*P = 0.001$). By Student's tests. Error bars indicate SEM. $n = 7$–10. (*D*–*F*) Kaplan–Meier survival analyses of metastatic setting study in mice with spontaneous lung metastases arising from orthotopic breast tumors, by log-rank tests. (*D*) Animal survival in mice with spontaneous E0771 lung metastases. The immunotherapy mixture improves median animal survival time by day 43 ($**P < 001$), and the combination with AMD3100 greatly extends the animal survival by curing four of seven mice ($*P < 0.0001$). $n = 7$. (*E*) Animal survival in mice with spontaneous MCa-M3C lung metastases. The immunotherapy mixture does not improve median animal survival time, but the combination with AMD3100 extends the animal survival by 76%, curing 2 of 10 mice ($*P < 0.001$). $n = 9$–10. (*F*) Animal survival in mice with spontaneous 4T1 lung metastases. The immunotherapy mixture does not improve median animal survival time, but the combination with AMD3100 extends the animal survival by 35% ($*P = 0.055$), curing 2 of 10 mice. $n = 9$–10.

Discussion

CXCR4 is a chemokine receptor frequently overexpressed by many solid tumors such as breast, colon, and prostate (38). High expression levels of CXCL12 and CXCR4 are predictive of poor prognosis in BC patients (39). CXCR4/CXCL12 signaling promotes CAF recruitment, activation, and matrix production in BCs, and tissue hypoxia induces CXCL12 and CXCR4 expression in both cancer cells and stromal cells through HIF1a activation (16). Signaling through CXCR4 in BCs also promotes VEGF-dependent angiogenesis, myeloid cell recruitment, tumor cell migration, and resistance to therapy (34, 36, 40–42).

Importantly, gradients of CXCL12, the chemotactic ligand of CXCR4, can attract cancer and other stromal cells and regulate their growth and migration at the metastatic sites (38, 43, 44). As such, blocking CXCR4 reduces the development of metastases (38, 45). Our data demonstrate that targeting CXCR4 can also improve the therapeutic efficacy of ICB in metastatic breast cancers.

Breast cancers and other highly desmoplastic tumors are generally poorly perfused and hypoxic, all contributing to poor drug delivery and effectiveness. The chemotactic and metastatic responses mediated by CXCR4 have been demonstrated in various solid cancers (38, 45–47). Furthermore, a recent study has shown that some CAFs can be immunosuppressive and that they may be driven by CXCR4/CXCL12 signaling to promote the recruitment and survival of regulatory T cells (32). Our results are consistent with Costa et al.'s (32) observation that CXCR4 signaling in the immunosuppressive αSMA+ CAFs can promote infiltration of FoxP3+ Tregs. However, future studies are needed to delineate the role of various cell types expressing αSMA. We may also be observing some reversal of immunosuppression related to hypoxia, which can promote CAF expression of TGF-β leading to exclusion of CD8+ T cells from the tumor parenchyma to restrain antitumor immunity following immunotherapy (7, 8). In addition, it has been demonstrated that the CXCL5/CXCR2 axis can promote recruitment of Gr1+ CD11b+ cells into the TME and further contribute to TGFβ1-mediated metastasis to the lung (30, 31, 48). Our observation that CXCR4 inhibition can decrease the expression of *Cxcl5* in αSMA+ cells, which consist of mostly CAFs, may point to a mechanism of CAF-driven recruitment of immunosuppressive CXCR2+ cells such as tumor-associated macrophages and neutrophils. As such, inhibiting CXCR4 could reprogram CAFs to down-regulate expression of prometastatic cytokines to reduce metastatic development and provide a more favorable outcome when combined with ICB.

This report characterizes T-lymphocyte exclusion, fibrosis, and immunosuppression in the metastases of breast cancers. Understanding the degree of fibrosis and how it influences the local tumor microenvironment in metastatic sites of BCs will provide valuable insights for the development of antimetastatic therapies. However, larger cohorts of human metastatic breast samples from different genetic subsets should be evaluated to help determine whether desmoplasia-targeting therapies such as angiotensin inhibitors (49, 50) and CXCR4 inhibitors (9, 51) that are safe and approved for other indications will benefit patients with late-stage metastatic disease, including metastasis with different histopathological growth patterns (52–55). Given that CXCR4 signaling is a key driver for tumor fibrosis and immunosuppression, it is reasonable to speculate that combining CXCR4 inhibition could potentially unleash further benefits of immunotherapy in mBC patients.

Materials and Methods

Immunohistochemistry studies were conducted on breast tissues from patients diagnosed with metastatic breast cancer at Brigham and Women's Hospital (BWH) in Boston. This study was approved by the Institutional Review Board at BWH. All patient samples were deidentified prior to the study. Orthotopic breast tumors were generated by implanting 200,000 cells into the third mammary fat pad of 6- to 8-wk-old female mice. For in vivo imaging studies, MCa-M3C cells were implanted in the αSMA-dsRed mice. For conditional knockout studies, we generated αSMA-dsRed/Cxcr4$^{flox/flox}$/C57 double-transgenic mice by crossing αSMA-dsRed mice with Cxcr4$^{flox/flox}$ mice. To induce deletion of *Cxcr4*, αSMA-dsRed/Cxcr4$^{flox/flox}$/C57 mice were injected daily with tamoxifen (10 mg/kg; Sigma) intraperitoneally for 2 wk before experiments. All animal procedures were carried out following the Public Health Service Policy on Humane Care of Laboratory Animals and approved by the Institutional Animal Care and Use Committee of the Massachusetts General Hospital. Experimental procedures are described in detail in *SI Appendix*.

ACKNOWLEDGMENTS. We thank Julia Kahn, Sylvie Roberge, and Carolyn Smith for technical assistance and Drs. Meenal Datta, Dan G. Duda, Dai Fukumura, Takahiro Heishi, Louis Larrouquere, Hao Liu, John Martin, Ethel Pereira, and David Tuveson for their help. This research was supported by grants from the National Foundation for Cancer Research; the Ludwig Center at Harvard; the Jane's Trust Foundation; National Cancer Institute (NCI) Grants P01-CA080124, R01-CA098706; R01-CA208205 and U01-CA224348; and the Department of Defense Breast Cancer Research Program Innovator Award W81XWH-10-1-0016 (to R.K.J.). R.K.J. is a recipient of Outstanding Investigator Award R35-CA197743 from the NCI. V.P.C. is a Fellow of the Life Sciences Research Foundation and was supported by Ruth L. Kirschstein National Research Service Award Postdoctoral Fellowship F32-CA073479 from the NIH and by a Misrock Postdoctoral Fellowship from the Misrock Foundation through the S. Leslie Misrock (1949) Frontier Research Fund for Cancer Nanotechnology. J.P. was supported by NIH Training Grant T32HL007627. I.X.C. was supported by a Gates Graduate Fellowship. M.R.N. was supported by Department of Defense Breast Cancer Research Program Postdoctoral Fellowship W81XWH-14-1-0034 and by a Simeon J. Fortin Charitable Foundation Postdoctoral Fellowship.

1. Schmid P, et al. (2018) Atezolizumab and nab-paclitaxel in advanced triple-negative breast cancer. *N Engl J Med* 379:2108–2121.
2. Emens LA (2018) Breast cancer immunotherapy: Facts and hopes. *Clin Cancer Res* 24: 511–520.
3. Ahn S, et al. (2012) The prognostic significance of tumor-associated stroma in invasive breast carcinoma. *Tumour Biol* 33:1573–1580.
4. de Kruijf EM, et al. (2011) Tumor-stroma ratio in the primary tumor is a prognostic factor in early breast cancer patients, especially in triple-negative carcinoma patients. *Breast Cancer Res Treat* 125:687–696.
5. Öhlund D, et al. (2017) Distinct populations of inflammatory fibroblasts and myofibroblasts in pancreatic cancer. *J Exp Med* 214:579–596.
6. Biffi G, et al. (2018) IL-1-induced JAK/STAT signaling is antagonized by TGF-beta to shape CAF heterogeneity in pancreatic ductal adenocarcinoma. *Cancer Discov* CD-18-0710.
7. Mariathasan S, et al. (2018) TGFβ attenuates tumour response to PD-L1 blockade by contributing to exclusion of T cells. *Nature* 554:544–548.
8. Tauriello DVF, et al. (2018) TGFβ drives immune evasion in genetically reconstituted colon cancer metastasis. *Nature* 554:538–543.
9. Feig C, et al. (2013) Targeting CXCL12 from FAP-expressing carcinoma-associated fibroblasts synergizes with anti-PD-L1 immunotherapy in pancreatic cancer. *Proc Natl Acad Sci USA* 110:20212–20217.
10. Acerbi I, et al. (2015) Human breast cancer invasion and aggression correlates with ECM stiffening and immune cell infiltration. *Integr Biol* 7:1120–1134.
11. Peranzoni E, Rivas-Caicedo A, Bougherara H, Salmon H, Donnadieu E (2013) Positive and negative influence of the matrix architecture on antitumor immune surveillance. *Cell Mol Life Sci* 70:4431–4448.
12. Stylianopoulos T, et al. (2012) Causes, consequences, and remedies for growth-induced solid stress in murine and human tumors. *Proc Natl Acad Sci USA* 109: 15101–15108.
13. Chauhan VP, et al. (2013) Angiotensin inhibition enhances drug delivery and potentiates chemotherapy by decompressing tumour blood vessels. *Nat Commun* 4:2516.
14. Barsoum IB, Smallwood CA, Siemens DR, Graham CH (2014) A mechanism of hypoxia-mediated escape from adaptive immunity in cancer cells. *Cancer Res* 74:665–674.
15. Pearce EL, et al. (2009) Enhancing CD8 T-cell memory by modulating fatty acid metabolism. *Nature* 460:103–107.
16. Noman MZ, et al. (2011) Microenvironmental hypoxia orchestrating the cell stroma cross talk, tumor progression and antitumor response. *Crit Rev Immunol* 31:357–377.
17. Jain RK (2014) Antiangiogenesis strategies revisited: From starving tumors to alleviating hypoxia. *Cancer Cell* 26:605–622.
18. Fukumura D, Kloepper J, Amoozgar Z, Duda DG, Jain RK (2018) Enhancing cancer immunotherapy using antiangiogenics: Opportunities and challenges. *Nat Rev Clin Oncol* 15:325–340.
19. Kodack DP, et al. (2017) The brain microenvironment mediates resistance in luminal breast cancer to PI3K inhibition through HER3 activation. *Sci Transl Med* 9:eaal4682.
20. Cancer Genome Atlas Network (2012) Comprehensive molecular portraits of human breast tumours. *Nature* 490:61–70.
21. Chen Y, et al. (2014) CXCR4 inhibition in tumor microenvironment facilitates anti-programmed death receptor-1 immunotherapy in sorafenib-treated hepatocellular carcinoma in mice. *Hepatology* 61:1591–1602.
22. Righi E, et al. (2011) CXCL12/CXCR4 blockade induces multimodal antitumor effects that prolong survival in an immunocompetent mouse model of ovarian cancer. *Cancer Res* 71:5522–5534.
23. Eck SM, Côté AL, Winkelman WD, Brinckerhoff CE (2009) CXCR4 and matrix metalloproteinase-1 are elevated in breast carcinoma–associated fibroblasts and in normal mammary fibroblasts exposed to factors secreted by breast cancer cells. *Mol Cancer Res* 7:1033–1044.
24. Gonda TA, Varro A, Wang TC, Tycko B (2010) Molecular biology of cancer-associated fibroblasts: Can these cells be targeted in anti-cancer therapy? *Semin Cell Dev Biol* 21: 2–10.

25. Raz Y, et al. (2018) Bone marrow-derived fibroblasts are a functionally distinct stromal cell population in breast cancer. *J Exp Med* 215:3075–3093.
26. Biffi G, Tuveson DA (2018) Deciphering cancer fibroblasts. *J Exp Med* 215:2967–2968.
27. Jain RK (2013) Normalizing tumor microenvironment to treat cancer: Bench to bedside to biomarkers. *J Clin Oncol* 31:2205–2218.
28. Trapani JA, Smyth MJ (2002) Functional significance of the perforin/granzyme cell death pathway. *Nat Rev Immunol* 2:735–747.
29. Minn AJ, et al. (2005) Genes that mediate breast cancer metastasis to lung. *Nature* 436:518–524.
30. Yang L, et al. (2008) Abrogation of TGF beta signaling in mammary carcinomas recruits Gr-1+CD11b+ myeloid cells that promote metastasis. *Cancer Cell* 13:23–35.
31. Bierie B, et al. (2009) Abrogation of TGF-beta signaling enhances chemokine production and correlates with prognosis in human breast cancer. *J Clin Invest* 119:1571–1582.
32. Costa A, et al. (2018) Fibroblast heterogeneity and immunosuppressive environment in human breast cancer. *Cancer Cell* 33:463–479.e10.
33. Joyce JA, Fearon DT (2015) T cell exclusion, immune privilege, and the tumor microenvironment. *Science* 348:74–80.
34. Hiratsuka S, et al. (2011) C-X-C receptor type 4 promotes metastasis by activating p38 mitogen-activated protein kinase in myeloid differentiation antigen (Gr-1)-positive cells. *Proc Natl Acad Sci USA* 108:302–307.
35. Kim HK, De La Luz Sierra M, Williams CK, Gulino AV, Tosato G (2006) G-CSF down-regulation of CXCR4 expression identified as a mechanism for mobilization of myeloid cells. *Blood* 108:812–820.
36. Jung K, et al. (2017) Targeting CXCR4-dependent immunosuppressive Ly6C^{low} monocytes improves antiangiogenic therapy in colorectal cancer. *Proc Natl Acad Sci USA* 114:10455–10460.
37. Whatcott CJ, et al. (2015) Desmoplasia in primary tumors and metastatic lesions of pancreatic cancer. *Clin Cancer Res* 21:3561–3568.
38. Müller A, et al. (2001) Involvement of chemokine receptors in breast cancer metastasis. *Nature* 410:50–56.
39. Mirisola V, et al. (2009) CXCL12/SDF1 expression by breast cancers is an independent prognostic marker of disease-free and overall survival. *Eur J Cancer* 45:2579–2587.
40. Guleng B, et al. (2005) Blockade of the stromal cell-derived factor-1/CXCR4 axis attenuates in vivo tumor growth by inhibiting angiogenesis in a vascular endothelial growth factor-independent manner. *Cancer Res* 65:5864–5871.
41. Marchesi F, et al. (2004) Increased survival, proliferation, and migration in metastatic human pancreatic tumor cells expressing functional CXCR4. *Cancer Res* 64:8420–8427.
42. Jung K, et al. (2017) Ly6Clo monocytes drive immunosuppression and confer resistance to anti-VEGFR2 cancer therapy. *J Clin Invest* 127:3039–3051.
43. Boimel PJ, et al. (2012) Contribution of CXCL12 secretion to invasion of breast cancer cells. *Breast Cancer Res* 14:R23.
44. Smith MCP, et al. (2004) CXCR4 regulates growth of both primary and metastatic breast cancer. *Cancer Res* 64:8604–8612.
45. Hassan S, et al. (2011) CXCR4 peptide antagonist inhibits primary breast tumor growth, metastasis and enhances the efficacy of anti-VEGF treatment or docetaxel in a transgenic mouse model. *Int J Cancer* 129:225–232.
46. Orimo A, et al. (2005) Stromal fibroblasts present in invasive human breast carcinomas promote tumor growth and angiogenesis through elevated SDF-1/CXCL12 secretion. *Cell* 121:335–348.
47. Richert MM, et al. (2009) Inhibition of CXCR4 by CTCE-9908 inhibits breast cancer metastasis to lung and bone. *Oncol Rep* 21:761–767.
48. DeNardo DG, et al. (2009) CD4(+) T cells regulate pulmonary metastasis of mammary carcinomas by enhancing protumor properties of macrophages. *Cancer Cell* 16:91–102.
49. Liu H, et al. (2017) Use of angiotensin system inhibitors is associated with immune activation and longer survival in nonmetastatic pancreatic ductal adenocarcinoma. *Clin Cancer Res* 23:5959–5969.
50. Pinter M, Jain RK (2017) Targeting the renin-angiotensin system to improve cancer treatment: Implications for immunotherapy. *Sci Transl Med* 9:eaan5616.
51. Lee EQ, et al. (2018) Phase I and biomarker study of plerixafor and bevacizumab in recurrent high-grade glioma. *Clin Cancer Res* 24:4643–4649.
52. Duda DG, et al. (2010) Malignant cells facilitate lung metastasis by bringing their own soil. *Proc Natl Acad Sci USA* 107:21677–21682.
53. Sledge GWJ, Jr (2016) Curing metastatic breast cancer. *J Oncol Pract* 12:6–10.
54. Stessels F, et al. (2004) Breast adenocarcinoma liver metastases, in contrast to colorectal cancer liver metastases, display a non-angiogenic growth pattern that preserves the stroma and lacks hypoxia. *Br J Cancer* 90:1429–1436.
55. Frentzas S, et al. (2016) Vessel co-option mediates resistance to anti-angiogenic therapy in liver metastases. *Nat Med* 22:1294–1302.